Arenium ions are not obligatory intermediates in electrophilic aromatic substitution

Boris Galabov[a,1], Gergana Koleva[a], Svetlana Simova[b], Boriana Hadjieva[a], Henry F. Schaefer III[c,1], and Paul von Ragué Schleyer[c,1]

[a]Department of Chemistry and Pharmacy, University of Sofia, Sofia 1164, Bulgaria; [b]Institute of Organic Chemistry with Centre of Phytochemistry, Laboratory Nuclear Magnetic Resonance, Bulgarian Academy of Sciences, Sofia 1113, Bulgaria; and [c]Center for Computational Quantum Chemistry and Department of Chemistry, University of Georgia, Athens, GA 30602

Edited* by Martin Saunders, Yale University, New Haven, CT, and approved May 28, 2014 (received for review March 18, 2014)

Our computational and experimental investigation of the reaction of anisole with Cl_2 in nonpolar CCl_4 solution challenges two fundamental tenets of the traditional S_EAr (arenium ion) mechanism of aromatic electrophilic substitution. Instead of this direct substitution process, the alternative addition–elimination (AE) pathway is favored energetically. This AE mechanism rationalizes the preferred *ortho* and *para* substitution orientation of anisole easily. Moreover, neither the S_EAr nor the AE mechanisms involve the formation of a σ-complex (Wheland-type) intermediate in the rate-controlling stage. Contrary to the conventional interpretations, the substitution (S_EAr) mechanism proceeds concertedly via a single transition state. Experimental NMR investigations of the anisole chlorination reaction course at various temperatures reveal the formation of tetrachloro addition by-products and thus support the computed addition–elimination mechanism of anisole chlorination in nonpolar media. The important autocatalytic effect of the HCl reaction product was confirmed by spectroscopic (UV-visible) investigations and by HCl-augmented computational modeling.

organic chemistry | reaction mechanisms | alternative computed routes | autocatalysis

Interest in the chemistry of electrophilic aromatic substitution reactions continues because of their widespread application for the production of a great variety of chemicals and materials (1–4). Electrophilic substitution, considered to be the most characteristic reaction of aromatic systems, is typically described in textbooks, monographs, and reviews by the two-stage S_EAr mechanism depicted in Fig. 1 (5–11). Arenium ion (σ-complex) intermediates are often ascribed to Wheland (9) inaccurately, since Pfeiffer and Wizinger (10) laid out the principles of such species for bromination in 1928. Following Brown and Pearsall (11), they are widely believed to have σ-complex structures. Arenium ions (σ-complexes) (9–11) are widely accepted to be obligatory intermediates and are used to rationalize *ortho*/*para* vs. *meta* position orientation preferences (6–11).

We now reinforce our challenges (12, 13) of this conventional "reaction mechanism paradigm" (14) by a combined computational and experimental study of the facile chlorination of anisole (methoxybenzene) with Cl_2 in CCl_4 solution (15, 16). We find that Fig. 1 is not the favored pathway. Instead, addition reactions of Cl_2 to anisole have the lowest activation energies (Fig. 2). Ready HCl elimination from the initially formed adducts leads to *ortho*- and *para*-chloroanisole as the predominate products. This addition–elimination (AE) mechanism (the historical antecedent to Fig. 1) (17–26) predicts the same positional orientation as the usually assumed direct substitution ("S_EAr") alternative. Instead of this classic S_EAr mechanism (Fig. 1), we find that direct concerted substitution, not involving an arenium ion, σ-complex ("Wheland") (9–11) intermediate, competes energetically with the AE route. Like some earlier computational studies on aromatic substitution (12, 13, 27, 28) (Rzepa H, www.ch.imperial.ac.uk/rzepa/blog/?p=2423, accessed March 10, 2013), our study finds no such intermediates in the direct substitution of anisole by Cl_2. A concerted mechanism without an arenium ion intermediate was computed at some levels for the related arene nitrosation, but reaction medium and counter ion effects were not considered. Gwaltney et al. (28) reported a single concerted transition state after reoptimizing all saddle points at CCSD(T)/6-31G(d,p) and modeling bulk solvation by the Onsager approximation, and Rzepa (www.ch.imperial.ac.uk/rzepa/blog/?p=2423, accessed March 10, 2013) also found a concerted transition state including a trifluoroacetate counterion. Instead, one-step reactions via single transition states take place (Fig. 2). Our experimental investigations of the chlorination of anisole in CCl_4 solution revealed tetrachloro by-products, which must have arisen by further reaction of intermediate dichloro-adducts. Both our UV-visible (UV-VIS) spectroscopic investigation and our theoretical modeling of this reaction clearly verified the autocatalytic effect of the HCl by-product, in harmony with Andrews and Keefer's (29, 30) early experimental kinetic studies of the chlorination of arenes, which found that HCl reduces the activation barriers significantly.

We also applied reliable theoretical methods to model a typical experimental example of the highly investigated S_EAr electrophilic aromatic halogenations, the electrophilic chlorination of anisole by molecular chlorine in simulated CCl_4 solution (15, 16). Although the elucidation of the classic S_EAr mechanism [Fig. 1, involving the initial formation of a π-complex, followed by a transition state leading to a σ-complex (arenium) intermediate in the rate-controlling stage, and, finally, proton loss from the ipso-position leading to the reaction product] is considered to be a triumph of physical organic chemistry (1, 31–37), an alternative addition–elimination pathway leading to substitution products has

Significance

Electrophilic substitution is universally regarded as the characteristic reaction of aromatic compounds. Arenium ions are widely accepted as obligatory intermediates in the two-stage (S_EAr) mechanism typically described in textbooks, monographs, and reviews. We now challenge this mechanistic paradigm. Our combined computational and experimental investigation of the exemplary halogenation of anisole with Cl_2 in CCl_4 finds that addition–elimination pathways compete with the direct substitution process and also account for the *ortho*–*para* orientation preferences easily. Moreover, the S_EAr processes do not involve arenium ion pair intermediates, but proceed instead via concerted one-stage single transition state routes. We question not only the generality of the accepted S_EAr mechanism, but also the involvement of arenium ion intermediates, when counter ions are present.

Author contributions: B.G., H.F.S., and P.v.R.S. designed research; G.K., S.S., and B.H. performed research; B.G., G.K., S.S., B.H., H.F.S., and P.v.R.S. analyzed data; B.G., H.F.S., and P.v.R.S. wrote the paper; and S.S. described the NMR results.

The authors declare no conflict of interest.

*This Direct Submission article had a prearranged editor.

[1]To whom correspondence may be addressed. E-mail: galabov@chem.uni-sofia.bg, ccq@uga.edu, or schleyer@uga.edu.

This article contains supporting information online at www.pnas.org/lookup/suppl/doi:10.1073/pnas.1405065111/-/DCSupplemental.

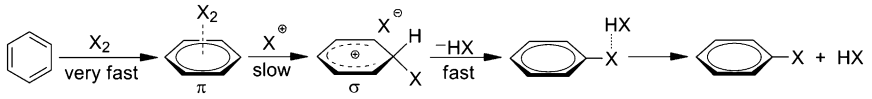

Fig. 1. Typical depiction of the arenium ion mechanism for S_EAr reactions.

been discussed since the 19th century (19–26, 38, 39). Nevertheless, it is commonly believed that the classic multistep S_EAr mechanism involving the formation of a σ-complex intermediate in the rate-controlling stage is the only mechanistic route to aromatic substitution products. Our present and previous (12, 13) results challenge the generality of such traditional interpretations. Although the initial stages of the alternative AE route seem unattractive because aromaticity is lost, many arenes are known experimentally to give addition products in considerable amounts (19–26, 38, 39). Thus, de la Mare (21, 25, 38, 39) demonstrated the formation of halogen adduct intermediates. Polybenzenoid hydrocarbons (PBHs) react with halogens to give isolable addition products, which then give substitution products easily by hydrogen halide elimination (23). Our computational investigations of arene bromination with molecular bromine (12) and sulfonation with SO_3 (13) provided clear evidence that the mechanisms of the inherent substitution reactions (i.e., uncatalyzed, gas phase, or weakly solvated) are concerted and do not involve the conventional σ-complex (or any other) intermediates. Moreover, the energetics of the bromination processes document the significance of competition between AE and direct substitution mechanisms leading to the same substitution products. Thus, the computed barrier in a simulated nonpolar (CCl_4) medium is 4 kcal/mol lower for Br_2 addition to benzene (followed by HBr elimination) than that for the direct substitution pathway to bromobenzene (12).

Previous theoretical studies of electrophilic aromatic halogenation processes have been based on the classic S_EAr mechanism, involving arenium ion intermediates (Fig. 1). Osamura et al.'s (40) Hartree-Fock computations of the $AlCl_3$-catalyzed electrophilic aromatic chlorination mechanism found an initial π-complex, a transition state preceding the intermediate σ-complex, and a second transition state leading to final products. Aluminum chloride was important as a Lewis acid catalyst throughout the process. $AlCl_3$ coordination polarizes Cl_2 and thereby assists its reaction with the arene. Rasokha and Kochi (41) considered the interaction of Br_2 with benzene and toluene in detail in their survey of theoretical and experimental data on the prereactive charge-transfer complexes in electrophilic aromatic substitutions. They argued that the structures and properties of the prereactive complexes provide important mechanistic insights for the S_EAr reactions. Wei et al.'s (42) theoretical study of the iodination of anisole by iodine monochloride at the B3LYP/6-311G* and MP2//B3LYP/6-311G* levels (B3LYP, Becke's three parameter hybrid functional, using the Lee-Yang-Parr correlation functional; MP2, second order Møller-Plesset perturbation theory computations) found that the highest energy transition state precedes the formation of an intermediate, which they interpreted to be a σ-complex. Instead, the structure of this complex represents a protonated iodobenzene. Volkov et al.'s MP2/LANL2DZ(d)+ study (43) of the chlorination of benzene established that dimers of group 13 metal halides catalyzed the processes more effectively. Optimized geometries of π- and σ-complexes as well as transition structures were reported. Theoretical investigations by Ben-Daniel et al. (44) and by Filimonov et al. (45) of the chlorination of benzene with Cl_2 (and other related processes) reported structural details of transition states purported to lead to the chlorobenzene product. Our reinvestigations revealed errors in major suppositions of both these studies. Our IRC computations show clearly that the transition states in question lead to 1,2 Cl_2–benzene addition products (rather than to chlorobenzene). Zhang and Lund (46) investigated the neat chlorination of toluene by Cl_2 experimentally and theoretically at B3LYP/cc-pVTZ(-f) [cc-pVTZ (-f), correlation consistent polarized triple-zeta without f-functions basis set]. Although we verified their reported geometry of the concerted transition state (figure 6 in ref. 46), our stability check revealed that its wavefunction is unstable. This casts doubt on their conclusions because of the homolysis vs. heterolysis issues. In contrast, all wavefunctions in our paper were checked and all are stable. Most prior theoretical studies of S_EAr halogenations did not consider the connections between transition states, intermediates, and products explicitly, as we have done.

Experimental findings not always have been in accord with the prevailing mechanistic assumption for aromatic halogenation: that arenium ion formation is the rate-limiting step. Thus, Olah et al. (47), Kochi and coworkers (48), and Fukuzumi and Kochi (49) have emphasized that substrate and positional selectivity are inconsistent (e.g., low toluene/benzene reactivity ratios but high toluene *ortho–para* vs. *meta* regiospecificity) for some electrophiles under certain conditions. This disparity indicates the existence of at least one other mechanistic pathway. It has been suggested that π-complexes may control product formation. Olah et al.'s (47) kinetics of the ferric chloride-catalyzed bromination of benzene and alkyl benzenes provided strong evidence for low substrate selectivity in the rate-determining step, which precedes the formation of a σ-complex intermediate (Fig. 1). High positional selectivity is governed by the transition state associated with the second step of the reaction.

However, our earlier study (50) examined the possible participation of π-complexes in the key mechanistic steps of S_EAr bromination reactions in detail but found no link between the energy of formation of these complexes and the overall reactivity. Although there is no doubt that π-complexes form easily (via essentially barrierless processes) in most S_EAr reactions after mixing the

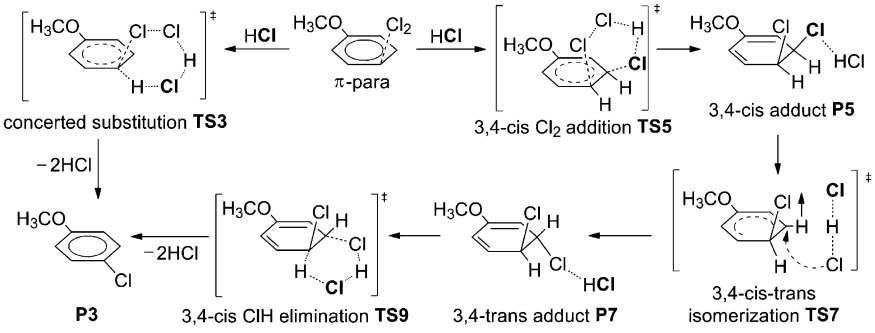

Fig. 2. The HCl-catalyzed concerted and addition–elimination pathways of *para*-chlorination of anisole in nonpolar media.

electrophile and the aromatic substrate, it is unlikely that these low-energy "bystander" structures influence rates of S_EAr reactions significantly. Thus, the lack of accord between substrate and positional selectivity, established by Olah et al. (47), Kochi and coworkers (48), and Fukuzumi and Kochi (49) may be due to other mechanistic differences. De la Mare and Bolton (21) and de la Mare (51) have stressed the plurality of aromatic substitution mechanisms, depending on the substrate and the conditions.

Reactive substrates are known to undergo uncatalyzed aromatic substitution in nonpolar solvents at room temperature. Thus, our computational investigations modeled Watson's careful experiments on the chlorination of anisole in CCl_4 at 25 °C (15, 16). His low conversion (25%) conditions for chlorophenol permitted more accurate determination of the initial product ratios (and avoided further Cl_2 additions to 4-chloroanisole, which ultimately gave 1,3,4,5,6-pentachloro-4-methoxycyclohexene). After introduction of gaseous Cl_2 into a CCl_4 solution of anisole for 1 h, the products were 4-chloroanisole (76%), 2-chloroanisole (13.6%), 2,6-dichloro anisole (2.1%), 2,4-dichloroanisole (3.0%), and 2,4,6-trichloroanisole (0.4%).

Analogous chlorinations of phenol, 2-methylphenol, and 2-chlorophenol in CCl_4 also have been carried out with high conversion rates at the reflux temperature (79 °C) (16). Chlorination of phenol with Cl_2 in CCl_4 has been reported by other groups (52, 53).

Methods

Our Gaussian 09 (54) computations used the 6-311+G(2d,2p) basis set (55, 56) with the B3LYP hybrid functional (57–59) and the Perdew–Burke–Ernzerhof (PBE) functional (60, 61) augmented with Grimme et al.'s (62) density functional theory with added Grimme's D3 dispersion corrections (DFT-D3). Single-point energies of all optimized structures were obtained with the B2-PLYP [double-hybrid density functional of Grimme (63)] and applying the D3 dispersion corrections. Intrinsic reaction coordinate (IRC) (64) computations connected the critical structures along the reaction path: reactants, transition states, intermediates, and products. The integral equation formalism of the polarizable continuum model (IEF-PCM) method (65) modeled solvent effects. Unrestricted broken symmetry (UBS B3LYP) computations on saddle-point structures along the potential energy surfaces gave the same energies as those from the restricted B3LYP method. Therefore, no diradical structures were involved along the reaction pathways investigated. All saddle-point wavefunctions were stable.

Extensive further testing assessed the methodological integrity of the B3LYP computations. We used the PBE method, which includes no contribution from exact exchange and thus is very different from B3LYP. All transition states were reoptimized with PBE and all intrinsic reaction coordinates were recomputed. As discussed below, the PBE results are qualitatively similar to those at B3LYP, strengthening the reliability of both methods for the present studies.

Our theoretical findings were supported by the results of parallel experimental investigations of chlorination reactions by NMR monitoring: ^1H (600.13 MHz) and ^{13}C (150.92 MHz) spectra were acquired during the course of the reactions. Unambiguous assignments of the signals were based on 1D

Table 1. Relative Gibbs free energies (Gibbs+E_{disp}) of species involved in the autocatalyzed by HCl anisole–Cl_2 reaction at B3LYP/6-311+G(2d,2p), PBE/6-311+G(2d,2p), and RB2PLYP/6-311+G(2d,2p)//RB3LYP/6-311+G(2d,2p) and for the uncatalyzed reaction at RB2PLYP/6-311+G(2d,2p)

Species	Description	B3LYP*, kcal/mol, catalyzed, gas phase	B3LYP*, kcal/mol, catalyzed, CCl_4	PBEPBE*, kcal/mol, catalyzed, CCl_4	B2PLYP//B3LYP*, kcal/mol, catalyzed, CCl_4	B2PLYP†, kcal/mol, uncatalyzed, CCl_4
π-ortho		2.63	2.81	1.20	2.98	2.99
π-para		2.76	2.86	1.53	3.26	3.23
TS1	*o* substitution	32.19	22.24	15.97	23.71	—
TS2	*m* substitution	39.65	32.14	25.09	34.58	—
TS3	*p* substitution	30.84	20.99‡	14.96	22.56§	—
TS4	2,3 addition	32.97 *cis* add.	21.00 *trans* add.	17.72 *cis* add.	22.08 *trans* add.	34.75 *cis* add.
TS4$_{meta}$¶	2,3 addition	39.19 *cis* add.	30.51 *trans* add.	24.58 *trans* add.	32.31 *trans* add.	—
TS5	3,4-*cis* addition	30.07	17.78	13.15	18.93	30.65
TS5$_{meta}$¶	3,4-*cis* addition	40.61	31.73	25.26	33.85	—
TS6	2,3-*cis–trans*	29.24	—	14.66	—	—
TS7	3,4-*cis–trans*	25.48	14.49§	11.73§	14.80§	21.21
TS7$_{meta}$¶	3,4-*cis–trans*	35.11	26.96	22.78	28.15	—
TS8	2,3-*cis* HCl eli.	17.15	10.44	6.35	11.51	16.85
TS8$_{meta}$¶	2,3 HCl eli.	35.56 *trans* eli.	20.13 *cis* eli.	14.05 *cis* eli.	21.55 *cis* eli.	25.86 *cis* eli.
TS9	3,4-*cis* HCl eli.	13.27	6.60	3.36	7.43	12.73
TS9$_{meta}$¶	3,4-*cis* HCl eli.	23.31	19.83	13.41	21.49	24.73
TS10	*cis–cis* rot.	—	10.61	8.20	7.73	5.21
TS11	*trans–trans* rot.	7.48	8.08	5.36	5.65	2.20
P1	*o* product	−21.45	−21.52	−22.75	−24.16	−27.47
P2	*m* product	−23.35	−22.80	−23.46	−25.26	−28.37
P3	*p* product	−23.47	−23.63	−23.21	−26.08	−28.28
P4	2,3-*cis* adduct	7.60	—	3.15	—	—
P5′	3,4-*cis* adduct	—	5.50	1.01	2.50	−0.42
P5′′	3,4-*cis* adduct	8.47	8.26	4.47	5.57	3.01
P5$_{meta}$‖	3,4-*cis* adduct	6.05	7.08	3.52	3.81	—
P6	2,3-*trans* adduct	2.10	2.42	−1.02	−0.33	−3.36
P6$_{meta}$‖	2,3-*trans* adduct	—	6.12	2.56	3.69	—
P7′	3,4-*trans* adduct	1.15	1.53	−0.32	−0.89	0.09
P7′′	3,4-*trans* adduct	5.11	5.18	2.06	3.09	−3.54
P7$_{meta}$‖	3,4-*trans* adduct	2.00	2.31	−0.69	−0.28	—

rot., rotation; eli., elimination; add., addition.

*Energies are relative to anisole, Cl_2, and HCl, except for the π-complexes, where the energies are relative to anisole and Cl_2.

†Only data for stable wave functions obtained for the uncatalyzed chlorination are shown in this column (see text for additional explanations). Energies are relative to anisole and Cl_2.

‡From B3LYP/6-311+G(2d,2p)//B3LYP/6-31+G(d,p) computations.

§Δ(G+E_{disp}) was determined from IEF-PCM (integral equation formalism of the polarizable continuum model) single-point computations at the gas-phase optimized structure.

¶High-energy transition states, leading to formation of adducts, in which the orientation of the HCl leads to formation of *m*-substituted product;

‖High-energy adducts, leading to *m*-substituted product formation.

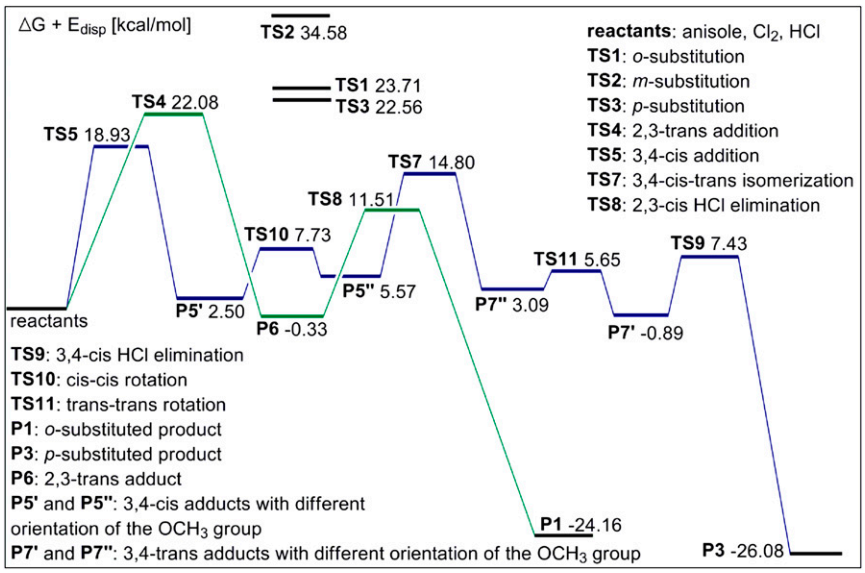

Fig. 3. Computed PES for anisole–Cl_2 reactions, catalyzed by HCl, in simulated CCl_4 solution at B2-PLYP+D3/6-311+G(2d,2p)//B3LYP/6-311+G(2d,2p). *Cis–trans* isomerization and elimination transition states, leading to formation of *m*-substituted product, are not included.

and 2D gradient-enhanced versions of correlation spectroscopy (COSY), total correlation spectroscopy (TOCSY), nuclear Overhauser and exchange spectroscopy (NOESY), heteronuclear single quantum coherence (HSQC) and heteronuclear multiple bond correlation (HMBC) experiments. Full details of the NMR experiments are provided in *SI Appendix*. The catalytic effect of HCl was confirmed experimentally by monitoring the reaction of anisole with Cl_2 in CCl_4, using UV-VIS spectroscopy.

Results and Discussion

Our computations of the potential energy surfaces (PES) of HCl-catalyzed anisole–Cl_2 reactions in simulated CCl_4 solution at B2-PLYP-D3/6-311+G(2d,2p)//B3LYP/6-311+G(2d,2p) model the experimental conditions closely (15, 16). Four competing processes were examined: direct substitutions at *ortho* [transition state (**TS1**)] and *para* (**TS3**) positions, as well as 2,3- and 3,4-*cis* additions of Cl_2. The vicinal 2,3- and 3,4-dichloro adducts undergo *cis–trans* isomerization followed by HCl elimination to give *ortho*- and *para*-substitution products. The potential energy surfaces obtained after full optimization of all structures and comprehensive IRC computations at the B3LYP/6-311+G(2d,2p) DFT level are presented in *SI Appendix*, Figs. S1 and S2. Comparisons of the energies of critical structures along the reaction paths in isolation (gas phase) and in simulated CCl_4 solvent (Table 1) show that the bulk solvent effect (despite low polarity of CCl_4) is quite significant for some reaction stages. The catalytic effect of HCl is illustrated by the theoretically evaluated transitions state energies for uncatalyzed and catalyzed processes (Table 1). The comparison was possible only for the AE routes because no stable wave functions for several TS energies (see Table 1) of the uncatalyzed direct substitution processes could be obtained. Note that the barriers for the rate-controlling stages of the catalyzed AE pathways are more than 10 kcal/mol lower than the barriers of the respective uncatalyzed processes.

Fig. 3 shows the evaluated potential energy surfaces and *SI Appendix*, Fig. S3 illustrates key PES saddle-point structures in simulated CCl_4 media. Fig. 3 reveals two extraordinary features. In contrast to traditional interpretations, the direct substitution pathways (both at the *ortho*- and at the *para*-positions) proceed through single concerted transition states (**TS1** and **TS3**) leading directly to products. No σ-complex arenium ion intermediates are involved in the reaction path, even as ion pairs. Low-energy π-complexes are formed at the initial step. The IRC computations backward from the first transition states end at three-component π-complexes (with free energies of formation about 7 kcal/mol higher than the initial reactants). These three-component π-complexes decompose easily into the usual two-component Cl_2–anisole complexes that have about 4 kcal/mol lower energy (Table 1). The forward IRC computations from the concerted transition states (**TS1** and **TS3**) lead to product complexes, which then transform into *ortho*- and *para*-substitution products. The results show that *para*-position attack is favored energetically (**TS3** energy, 22.56 kcal/mol) over that of the *ortho* position (**TS1** energy, 23.7 kcal/mol). As expected, the *meta*-substitution barrier (**TS2**, 34.6 kcal/mol) is distinctly higher than that of *ortho* and *para*. The structures of these direct substitution transition states (*SI Appendix*, Fig. S3) show no significant bond length changes in the aromatic ring. The CC bond lengths neighboring the position of attack are elongated only slightly, and the ring preserves its aromatic character. Thus, these transition states do not have arenium-type cyclohexadienyl geometries.

The results reveal that AE routes are favored over direct substitution. The most pronounced difference (3.6 kcal/mol lower barrier) is for the processes leading to *p*-chloroanisole, the principal reaction product (Fig. 3). The AE route also is favored, although to a lesser extent (1.6 kcal/mol), for *ortho* substitution. Overall, the data obtained suggest that AE pathways dominate over concerted substitution in anisole chlorination.

The structures of the rate-determining addition transition states (**TS4**, **TS5**) are highly unsymmetrical with one C–Cl bond almost formed, whereas the other chlorine atom is still quite far from its eventual bonding site (*SI Appendix*, Fig. S3). The HCl catalyst facilitates the addition of the second chlorine atom to the ring (**TS5**; Fig. 2 and *SI Appendix*, Fig. S3; see Table 1), by lowering the transition state electronic energy considerably, compared to the uncatalyzed process. The subsequent barriers (**TS7**–**TS9**) along the AE routes shown in Fig. 3 have lower energies. The *cis–trans* isomerization process (**TS7**) is preceded and followed by the facile

Table 2. Ratios (in percent, relative to unreacted anisole) of reaction products from the chlorination of anisole in CCl_4 as determined by NMR

	1	2	3	4	5
Mixture 1*	100	12	1.0	0.8	0.6
Mixture 2†	100	74	3.7	2.4	3.0
Mixture 3‡	100	115	15.5	5.8	7.4
Mixture 4§	100	114	14.0	5.2	7.2

1, anisole; 2, *p*-chloroanisole; 3, *o*-chloroanisole; 4 and 5, by-products formed during the chlorination of anisole in CCl_4 (details in *SI Appendix*).
*0.01 mol/L anisole + Cl_2 (25 °C).
†0.05 mol/L anisole + Cl_2 (25 °C).
‡0.1 mol/L anisole + Cl_2 (25 °C).
§0.1 mol/L anisole + Cl_2 (5 °C).

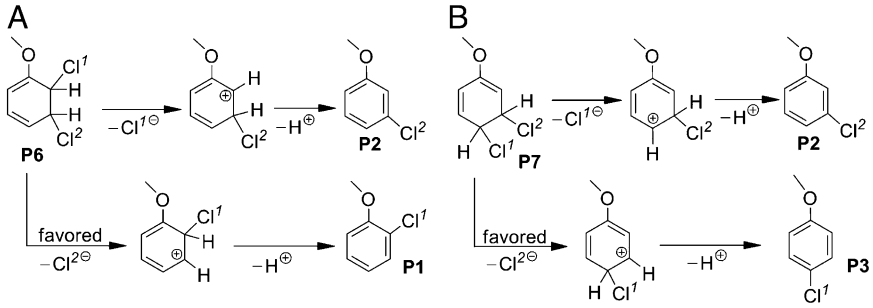

Fig. 4. Orienting methoxy group-carbocation conjugation effects explaining the HCl elimination preferences leading to (*A*) *ortho* and (*B*) *para* (rather than to *meta*) substitution products of anisole.

rotation of the methoxy groups (**TS10** and **TS11**; *SI Appendix*, Fig. S3). The 3,4-addition–elimination pathway yielding *para*-chloroanisole (**P3** via **TS7**, **P7**, and **TS9**) is preferred over the *ortho*-chloroanisole (**P1**) AE sequence (via **P6** and **TS8**). The result is in qualitative harmony with the experimentally observed greater *para*- than *ortho*-chloroanisole product yields (Table 2).

The AE mechanism explains the *ortho* and *para* orientation effect of the electron-donating methoxy group simply by the expected preferential stabilization of the transition states for HCl elimination, as illustrated in Fig. 4. Thus, the partial positive charges arising during HCl elimination (**TS8** and **TS9**; *SI Appendix*, Fig. S3) are stabilized by resonance conjugation with the methoxy group only in one of the two alternative TSs. In Fig. 4, the favored processes involve initial loss of the chlorides labeled Cl^2. Thus, HCl elimination from the 2,3-*trans* dichoro anisole adduct (**P6**) gives *ortho*- rather than *meta*-chloroanisole (Fig. 4*A*). Preferential HCl elimination from the 3,4-*trans* dichoro anisole adduct (**P7**) gives *para*- rather than *meta*-chloroanisole (Fig. 4*B*). Indeed, only traces of *meta*-substitution product were found in the Watson experiments (15, 16).

These qualitative interpretations are clearly supported by the computed energies of the HCl elimination processes (Table 1). The low-lying relative energy of **TS9** for 3,4 elimination is just 7.43 kcal/mol (B2PLYP//B3LYP; Fig. 3), whereas the energies of the two transition states leading to *meta*-substituted products are 21.55 kcal/mol ($\mathbf{TS8_{meta}}$) and 21.49 ($\mathbf{TS9_{meta}}$). As shown in Fig. 3, the energy of **TS8** is 11.51 kcal/mol for 2,3 elimination leading to the *ortho*-substitution product.

The results of the alternative PBE functional computations (Table 1) correspond well with the B2PLYP//B3LYP/6-311+G(2d,2p) data. Whereas the PBE/6-311+G(2d,2p) transition state energy estimates are typically lower than those at B2PLYP+D//B3LYP/6-311+G(2d,2p), the two sets of TS energies correlate well (coefficient $r = 0.973$) and support the mechanistic conclusions reached for anisole chlorination. Notably, these two quite different types of DFT functionals yield quite similar overall potential energy surface features.

The theoretical results were verified by a series of NMR studies of the reaction of anisole and Cl_2 in CCl_4 solution, using Watson's conditions (15, 16). Moreover, because the reaction at 25 °C was quite fast, we carried out in situ experiments at 5 °C and at −10 °C directly in the NMR tubes by making ^{1}H NMR measurements at intervals over extended periods of time. Full details of the experiments are provided in *SI Appendix*. As stated above, various 1D and 2D NMR (^{1}H and ^{13}C) techniques were used to analyze the mixture of reaction products. The reaction with Cl_2 at 25 °C (mixtures 3 and 4, Table 2) is complete in less than 5 min. Further product composition does not change with time, followed up to 1 wk. In *SI Appendix*, Figs. S6–S15 display representative NMR spectra of the product mixtures.

More than 25 products from the partial reaction of anisole (**1**) with Cl_2 were detected in the mixtures by means of the CH_3O-group ^{1}H and ^{13}C peaks present in the HSQC spectra in the 3.4–4.0 ppm proton and 50–60 ppm carbon chemical shift ranges. The following compounds were identified: substitution products *para*-chloroanisole (**2**) and *ortho*-chloroanisole (**3**) and the double Cl_2 addition products, **4** and **5** (both of which have four chlorines). The relative ratios of the reaction products were determined (within 1%, relative to the remaining unreacted anisole, Table 2). Three diastereomers are possible for the addition product **4** that could not be distinguished on the basis of the experimental NMR data (details in *SI Appendix*). The structure shown in *SI Appendix*, Fig. S4 has the lowest energy among the three possible diastereomers according to B2PLYP+D3/6-311+G(2d,2p) computations (*SI Appendix*, Table S3). The initial concentration of anisole as well as the mixing procedure of the components in CCl_4 seems to influence the product ratios, but **2** always predominated. Although there were a number of unidentified products in smaller amounts, the NMR data do not reveal with certainty the presence of a detectable amount of any dichloro product formed by addition of only one molecule of chlorine to anisole.

However, our NMR results provide compelling evidence that addition reactions do take place during the interaction of anisole with molecular chlorine in CCl_4 solution. The tetrachlorinated products (**4** and **5**, *SI Appendix*, Fig. S4) we identified can be obtained only following initial additions of a single Cl_2 to anisole. The very low barriers for the elimination processes [7.43 kcal/mol for the 3,4-*cis* HCl elimination (**TS9**) and 11.51 kcal/mol for the 2,3-*cis* HCl elimination (**TS8**); Fig. 3], however, favor the pathways to substitution products, thus obviating the chance to detect the intermediate Cl_2 monoaddition products. In contrast, the tetrachloro addition products we obtained are quite stable and do not change during the course of the reaction. The NMR findings provide clear experimental confirmation that Cl_2 addition processes do take place during anisole chlorination, in remarkable agreement with the reported theoretical results on the reaction mechanism.

The catalytic effect of the HCl reaction product also was confirmed experimentally. We followed the reaction using UV-VIS spectroscopy at 25 °C in CCl_4 solution containing a large excess of anisole with respect to the chlorinating agent (at least 6:1 molar ratio). The consumption of the Cl_2 reactant was monitored by means of its absorption band at 330 nm. The course of the reaction in the absence of excess HCl is illustrated in *SI Appendix*, Fig. S5*A*. *SI Appendix*, Fig. S5*B* shows the pronounced catalytic effect when extra HCl was added to the CCl_4 solvent before introducing the Cl_2 reactant: The consumption of Cl_2 in the presence of extra catalyst is at least five times faster. As discussed already, these results are in harmony with the early kinetic findings of Andrews and Keefer for the chlorination of aromatic hydrocarbons in different solvents (29, 30). These authors established that the chlorination of pentamethylbenzene in CCl_4 is first order in hydrocarbon and chlorine and mixed first and second order with respect to HCl (30). The chlorination of toluene with molecular chlorine in ethylene dichloride was found to be first order with respect to hydrocarbon, chlorine, and HCl (29). In our experiments the rate enhancement observed in case B was due simply to the availability of more catalyst. The energetics of the reaction, however, are identical for both cases A and B and reflect a catalyzed process, pure autocatalysis in case A and combined autocatalytic and added catalyst effects in case B.

Our new theoretical and experimental investigations of the pathways and energies of anisole–Cl_2 reactions provide dramatic insights into electrophilic aromatic substitution mechanisms. The computational results reveal the involvement of two alternative reaction pathways, an addition–elimination sequence and a direct

concerted mechanism. The addition–elimination pathways are more favorable (the barriers are lower by 1.6–3.6 kcal/mol) and also result in the well-known orientational preference for *ortho*- and *para*-substituted anisole derivatives. The *ortho*/*para* orientation effect of the methoxy substituent is the natural consequence of the preferential stabilizing influence of the OCH_3 group. Moreover, no arenium σ-complex (or any other similar intermediate) is found along the reaction path for direct substitution. Experimentally, NMR elucidation of the anisole chlorination products provides clear evidence for the formation of addition products during the process, in harmony with the theoretical predictions. Autocatalysis by the HCl reaction product leads to significant lowering of reaction barriers.

ACKNOWLEDGMENTS. The research in Georgia was supported by the US National Science Foundation, Grants CHE-1361178 (to H.F.S.) and CHE-1057466 (to P.v.R.S.). The research in Sofia was supported by European Union Grant FP7-REGPOT-2011-1 (project BeyondEverest) and Bulgarian National Science Fund, Grant DRNF02-13/2009.

1. Godula K, Sames D (2006) C-H bond functionalization in complex organic synthesis. *Science* 312(5770):67–72.
2. Allemann O, Duttwyler S, Romanato P, Baldridge KK, Siegel JS (2011) Proton-catalyzed, silane-fueled Friedel-Crafts coupling of fluoroarenes. *Science* 332(6029):574–577.
3. Phipps RJ, Gaunt MJ (2009) A meta-selective copper-catalyzed C–H bond arylation. *Science* 323(5921):1593–1597.
4. Dong C, et al. (2005) Tryptophan 7-halogenase (PrnA) structure suggests a mechanism for regioselective chlorination. *Science* 309(5744):2216–2219.
5. Taylor R (1990) *Electrophilic Aromatic Substitution* (Wiley, New York).
6. Brouwer DM, Mackor EL, MacLean C (1970) Carbonium Ions, eds Olah GA, Schleyer PvR (Wiley-Interscience, New York), Vol 2.
7. Koptyug VA (1984) *Arenium Ions-Structure and Reactivity* (Springer, Heidelberg), pp 1–227.
8. Hubig SM, Kochi JK (2000) Structure and dynamics of reactive intermediates in reaction mechanisms. σ- and π-complexes in electrophilic aromatic substitutions. *J Org Chem* 65(21):6807–6818.
9. Wheland GW (1942) A quantum mechanical investigation of the orientation of substituents in aromatic molecules. *J Am Chem Soc* 64(4):900–908.
10. Pfeiffer P, Wizinger R (1928) Zur theorie der halogensubstitution [On the theory of halogen substitution]. *Justus Liebigs Ann Chem* 461(1):132–154. German.
11. Brown HC, Pearsall HW (1952) The action of the catalyst couple aluminum chloride–hydrogen chloride on toluene at low temperatures; the nature of Friedel–Crafts complexes. *J Am Chem Soc* 74(1):191–195.
12. Kong J, et al. (2011) The inherent competition between addition and substitution reactions of Br_2 with benzene and arenes. *Angew Chem Int Ed* 50(30):6809–6813.
13. Koleva G, Galabov B, Kong J, Schaefer HF, Schleyer PvR (2011) Electrophilic aromatic sulfonation with SO_3: Concerted or classic S_EAr mechanism? *J Am Chem Soc* 133(47): 19094–19101.
14. Sakic D, Vrcek V (2012) Prereactive complexes in chlorination of benzene, triazine, and tetrazine: A quantum chemical study. *J Phys Chem A* 116(4):1298–1306.
15. Watson WD (1974) Chlorination of phenols with chlorine and tert-butyl hypochlorite. Comparison. *J Org Chem* 39(8):1160–1164.
16. Watson WD (1982) Formation of nonaromatic products in the chlorination of simple substituted aromatic ethers. *J Org Chem* 47(27):5270–5276.
17. de Queiroz JF, et al. (2006) Electrophilic aromatic nitration: Uunderstanding its mechanism and substituent effects. *J Org Chem* 71(16):6192–6203.
18. Baciocchi E, Mandolini E (1987) The model for the transition state of electrophilic aromatic substitutions: σ-Complex or excited charge-transfer complex? A mise au point. *Tetrahedron* 43(17):4035–4041.
19. Holleman AF (1925) Some factors influencing substitution in the benzene ring. *Chem Rev* 1(2):187–230.
20. Price CC (1941) Substitution and orientation in the benzene ring. *Chem Rev* 29(1):37–67.
21. De la Mare PBD, Bolton R (1966) *Electrophilic Additions to Unsaturated Systems* (Elsevier, New York), pp 241–251.
22. Jang KS, Shin HY, Chi DY (2008) Electrophilic aromatic addition reaction (Ad_EAr) to anthracene. *Tetrahedron* 64(24):5666–5671.
23. Duan S, et al. (2000) Halogenations of anthracenes and dibenz[a,c]anthracene with N-bromosuccinimide and N-chlorosuccinimide. *J Org Chem* 65(10):3005–3009.
24. Mayo FR, Hardy WB (1952) The bromination of naphthalene. *J Am Chem Soc* 74(4): 911–917.
25. De la Mare PBD (1974) Pathways in electrophilic aromatic substitutions. Cyclohexadienes and related compounds as intermediates in halogenation. *Acc Chem Res* 7(11): 361–368.
26. Ingold CK (1969) *Structure and Mechanism in Organic Chemistry* (Cornell Univ Press, New York), Chap 6, pp 221–306.
27. Skokov S, Wheeler RA (1999) Oxidative aromatic substitutions: Hartree–Fock/density functional and ab initio molecular orbital studies of benzene and toluene nitrosation. *J Phys Chem A* 103(21):4261–4269.
28. Gwaltney SR, Rasokha SV, Head-Gordon M, Kochi JK (2003) Charge-transfer mechanism for electrophilic aromatic nitration and nitrosation via the convergence of (ab initio) molecular-orbital and Marcus–Hush theories with experiments. *J Am Chem Soc* 125(11): 3273–3283.
29. Andrews LJ, Keefer RM (1959) The influence of solvent on the rate of aromatic chlorination. *J Am Chem Soc* 81(5):1063–1067.
30. Andrews LJ, Keefer RM (1957) The chlorination of aromatic hydrocarbons in carbon tetrachloride and in trifluoroacetic acid. *J Am Chem Soc* 79(19):5169–5174.
31. Carey FA, Sundberg RJ (2007) *Advanced Organic Chemistry, Part A, Structure and Mechanisms* (Springer, New York), Chap 10, pp 579–629.
32. Smith MB, March J (2013) *March's Advanced Organic Chemistry Reactions, Mechanisms and Structure* (Wiley, New York).
33. Streitwieser A (1961) *Molecular Orbital Theory for Organic Chemists* (Wiley, New York).
34. Bachrach SM (2014) *Computational Organic Chemistry* (Wiley, Hoboken, NJ).
35. Olah GA (1971) Aromatic substitution. XXVIII. Mechanism of electrophilic aromatic substitutions. *Acc Chem Res* 4(7):240–248.
36. Ridd JH (1971) Mechanism of aromatic nitration. *Acc Chem Res* 4(7):248–253.
37. Olah GA, Malhotra R, Narang SC (1989) *Nitration. Structure and Mechanisms* (VCH, New York).
38. De la Mare PBD, Johnson MD, Lomas JS, del Olmo VS (1966) The kinetics and mechanisms of aromatic halogen substitution. Part XXIV. The stereochemistry of addition of chlorine to naphthalene. *J Chem Soc B* 827–833.
39. De la Mare PBD, et al. (1969) Kinetics and mechanisms of aromatic halogen substitution. Part XXVIII. Environmental effects on rates and products of chlorination of some aromatic hydrocarbons. *J Chem Soc B* 717–724.
40. Osamura Y, Terada K, Kobayashi Y, Okazaki R, Ishiyama Y (1999) A molecular orbital study of the mechanism of chlorination reaction of benzene catalyzed by Lewis acid. *J Mol Struct Theochem* 461–462:399–416.
41. Rosokha SV, Kochi JK (2002) The preorganization step in organic reaction mechanisms. Charge-transfer complexes as precursors to electrophilic aromatic substitutions. *J Org Chem* 67(6):1727–1737.
42. Wei Y, et al. (2005) Theoretical study of the iodination of methoxybenzene by iodine monochloride. *J Phys Org Chem* 18(7):625–631.
43. Volkov AN, Timoshkin AY, Suvorov AV (2005) Pathways of electrophilic aromatic substitution reactions catalyzed by group 13 trihalides: An ab initio study. *Int J Quantum Chem* 104(2):256–260.
44. Ben-Daniel R, de Visser SP, Shaik S, Neumann R (2003) Electrophilic aromatic chlorination and haloperoxidation of chloride catalyzed by polyfluorinated alcohols: A new manifestation of template catalysis. *J Am Chem Soc* 125(40):12116–12117.
45. Filimonov VD, Poleshchuk OK, Krasnokutskaya EA, Frenking G (2011) DFT investigation of the thermodynamics and mechanism of electrophilic chlorination and iodination of arenes. *J Mol Model* 17(11):2759–2771.
46. Zhang M, Lund CRF (2002) An experimental and computational study of solvent effects in toluene chlorination. *J Phys Chem A* 106(43):10294–10301.
47. Olah GA, Kuhn SJ, Flood SH, Hardie BA (1964) Aromatic substitution. XIV. Ferric chloride catalyzed bromination of benzene and alkylbenzenes with bromine in nitromethane solution. *J Am Chem Soc* 86(6):1039–1044.
48. Vasiliev AV, Lindeman SV, Kochi JK (2002) Molecular structures of the metastable charge-transfer complexes of benzene (and toluene) with bromine as the pre-reactive intermediates in electrophilic aromatic bromination. *New J Chem* 26:582–592.
49. Fukuzumi S, Kochi JK (1982) Transition-state barrier for electrophilic reactions. Solvation of charge-transfer ion pairs as the unifying factor in alkene addition and aromatic substitution with bromine. *J Am Chem Soc* 104(26):7599–7609.
50. Koleva G, Galabov B, Wu J, Schaefer HF, Schleyer PvR (2009) Electrophile affinity: A reactivity measure for aromatic substitution. *J Am Chem Soc* 131(41):14722–14727.
51. De la Mare PBD (1976) *Electrophilic Halogenations* (Cambridge Univ Press, Cambridge, UK).
52. Harvey DR, Norman ROC (1961) The ortho:para-ratio in aromatic substitution. Part II. Chlorination with t-butyl hypochlorite. *J Chem Soc* 3604–3610.
53. Kennard WW, Matthews DN (1960) The para:ortho ratio in the monochlorination of phenol. *Aust J Chem* 13(2):317–320.
54. Frisch MJ, et al. (2009) *GAUSSIAN09, Revision A. 02* (Gaussian, Wallingford, CT).
55. Curtiss LA, et al. (1995) Extension of Gaussian-2 theory to molecules containing third-row atoms Ga-Kr. *J Chem Phys* 103(14):6104–6113.
56. Clark T, Chandrasekhar J, Spitznagel GW, Schleyer PvR (1983) Efficient diffuse function-augmented basis sets for anion calculations. III. The 3-21+G basis set for first-row elements, Li–F. *J Comput Chem* 4(3):294–301.
57. Becke AD (1993) Density-functional thermochemistry. III. The role of exact exchange. *J Chem Phys* 98(7):5648–5653.
58. Becke AD (1996) Density-functional thermochemistry. IV. A new dynamical correlation functional and implications for exact-exchange mixing. *J Chem Phys* 104(3):1040–1046.
59. Lee CT, Yang WT, Parr RG (1988) Development of the Colle-Salvetti correlation-energy formula into a functional of the electron density. *Phys Rev B* 37:785–789.
60. Perdew JP, Burke K, Ernzerhof M (1996) Generalized gradient approximation made simple. *Phys Rev Lett* 77:3865–3868.
61. Perdew JP, Burke K, Ernzerhof M (1997) Errata: Generalized gradient approximation made simple. *Phys Rev Lett* 78:1396.
62. Grimme S, Antony J, Ehrlich S, Krieg H (2010) A consistent and accurate ab initio parametrization of density functional dispersion correction (DFT-D) for the 94 elements H-Pu. *J Chem Phys* 132(15):154104.
63. Grimme S (2006) Semiempirical hybrid density functional with perturbative second-order correlation. *J Chem Phys* 124(3):034108.
64. Fukui K (1981) The path of chemical reactions – the IRC approach. *Acc Chem Res* 14(12): 363–368.
65. Tomasi J, Mennucci B, Cammi R (2005) Quantum mechanical continuum solvation models. *Chem Rev* 105(8):2999–3094.